# THEODORSEN'S AND GARRICK'S COMPUTATIONAL AEROELASTICITY, REVISITED

#### **Boyd Perry, III**

NASA – Langley Research Center Hampton, Virginia 23681-2199 USA boyd.perry.iii@nasa.gov

Keywords: Flutter; NACA Reports 496, 685, 741; Theodore Theodorsen; I.E. Garrick

**Abstract:** This paper describes a multiyear effort to recompute all of the numerical flutter results contained in Theodore Theodorsen's and I.E. Garrick's ("T&G's") groundbreaking trilogy of National Advisory Committee for Aeronautics technical reports on aeroelastic flutter (NACA Reports 496, 685, and 741). The paper includes overviews of T&G's aeroelastic equations and solution methods, comparisons between the original and recomputed numerical results, and instances of errors and tripping points (potentials for confusing the reader) in the original NACA reports.

#### 1 INTRODUCTION

In 1934, starting from first principles, Theodore Theodorsen laid out the theory of aeroelastic flutter for a typical section with three degrees of freedom and provided a method for its practical solution [1]. At the time, this solution method offered the only means of solving the flutter problem in an exact closed-form way. To borrow today's terminology and retroactively apply it to 1934, it can be argued that reference 1 was the original paper on computational aeroelasticity, the only differences between the original and today's variations being the accuracy and fidelity of their respective structural and unsteady aerodynamic representations. There were follow-on papers in 1938 [2] and 1942 [3] co-authored with I.E. Garrick.

In the year 2000 in an Engineering Note, Zeiler [4] made generally known that references 1-3, as well as early aeroelasticity texts [5, 6], contained numerical errors in some of their numerical examples. It is not surprising that such errors exist because (especially in the cases of refs. 1-3, written in the 1930s and early 1940s) all calculations were computed "by hand" with pencil, paper, slide rules, and mechanical calculators called comptometers. The theory in references 1-3 is flawless, but the computational resources of the time (humans with job title "computer") were inherently unreliable.

Because these foundational papers and texts are often used in graduate courses on aeroelasticity, Zeiler recommended that an effort be undertaken to employ the computational resources available today (digital computers) to recompute the example problems in these early works and to publish the results to provide a complete and error-free set of numerical examples.

The purpose of the present paper is to report on a multiyear effort that follows Zeiler's recommendation: to revisit references 1-3 and recompute all the numerical examples in these three

foundational NACA reports. For each of the NACA reports, the recomputations were performed using the solution method specific to that report. The recomputations were spot checked using current-day flutter solution methods. To date, recomputations have been completed for references 1 and 2 (with results appearing in refs. 7 and 8) and have begun for reference 3.

The remainder of this paper is arranged as follows:

Section 2 contains nomenclature;

Section 3 outlines the theoretical development of the aeroelastic equations of motion for a typical section with degrees of freedom torsion, aileron deflection, and bending;

Section 4 describes the solution methods employed in each of the three foundational papers – a different method for each of references 1, 2, and 3;

Section 5 presents some tripping points (aspects of the original papers that have the potential to cause confusion) found during the reading of references 1, 2, and 3;

Section 6 presents representative comparisons of T&G's original and recomputed results;

Section 7 contains concluding remarks.

For simplicity, for the remainder of this paper references 1-3 will be referred to, respectively, as "NACA 496," "NACA 685," and "NACA 741."

The title of the present paper is a nod to the title of reference 4.

#### 2 NOMENCLATURE

The symbols in this list are either identical to or consistent with the symbols used in references 1, 2, and 3.

- $A_{ij}$  ij-th coefficient in the equations of motion, complex
- a nondimensional distance from midchord to e.a., positive aft
- b semichord, ft
- $C_h$  stiffness in wing deflection, per unit length
- $C_{\alpha}$  torsional stiffness of wing about e.a., per unit length
- $C_{\beta}$  torsional stiffness of aileron about hinge, per unit length
- c nondimensional distance from midchord to aileron hinge, positive aft
- e base of natural logarithms
- $g_h$  structural damping coefficient for flexure mode
- $g_{\alpha}$  structural damping coefficient for torsion mode
- $g_{\beta}$  structural damping coefficient for aileron deflection mode
- h vertical deflection degree of freedom, positive down

- $h_0$  infinitesimal amplitude of h, positive down
- *i* square root of -1
- $I_{ij}$  imaginary part of  $A_{ij}$
- k reduced frequency,  $\omega b/v$
- $k_f$  flutter reduced frequency,  $\omega_f b/v_f$
- M mass of wing per unit length
- $R_{ij}$  real part of  $A_{ij}$
- $r_r$  nondimensional reference length
- $r_{\alpha}$  nondimensional radius of gyration of wing-aileron, referred to  $\alpha$
- $r_{\beta}$  nondimensional radius of gyration of aileron, referred to c
- $T_i$  constants resulting from the integration of velocity potentials, functions of c and a
- v velocity, fps
- $v_f$  flutter velocity, fps
- X nondimensional quantity resulting from normalizing equations of motion,  $\frac{1}{\kappa} \left( \frac{br_r \omega_r}{vk} \right)^2$
- $x_{\alpha}$  nondimensional distance from e.a. to c.g. of wing-aileron, positive aft
- $x_{\beta}$  nondimensional distance from aileron hinge to c.g. of aileron, positive aft
- $\alpha$  torsion degree of freedom, positive leading edge up
- $\alpha_0$  infinitesimal amplitude of  $\alpha$ , positive leading edge up
- $\beta$  aileron deflection degree of freedom, positive trailing edge down with respect to wing
- $\beta_0$  infinitesimal amplitude of  $\beta$ , positive trailing edge down with respect to wing
- $\kappa$  mass ratio,  $\frac{\pi \rho b^2}{M}$
- $\rho$  mass of air per unit volume
- $\xi$  modal-coupling factor
- $\varphi_0$  phase angle of  $\alpha$  with respect to an unspecified reference, radians
- $\varphi_1$  phase angle of  $\beta$  with respect to an unspecified reference, radians
- $\varphi_2$  phase angle of h with respect to an unspecified reference, radians
- $\omega$  circular frequency, radians per second, rps
- $\omega_f$  flutter frequency, rps
- $\omega_h$  natural frequency of wing-flexure mode, rps
- $\omega_r$  reference frequency, rps
- $\omega_{\alpha}$  natural frequency of wing-torsion mode, rps
- $\omega_{\beta}$  natural frequency of aileron-deflection mode, rps
- $\Omega_h$  square of nondimensional frequency ratio,  $\left(\frac{\omega_h}{\omega_r r_r}\right)^2$
- $\Omega_{\alpha}$  square of nondimensional frequency ratio,  $\left(\frac{\omega_{\alpha}r_{\alpha}}{\omega_{r}r_{r}}\right)^{2}$
- $\Omega_{\beta}$  square of nondimensional frequency ratio,  $\left(\frac{\omega_{\beta}r_{\beta}}{\omega_{r}r_{r}}\right)^{2}$

#### Abbreviations:

c.g. center of gravity

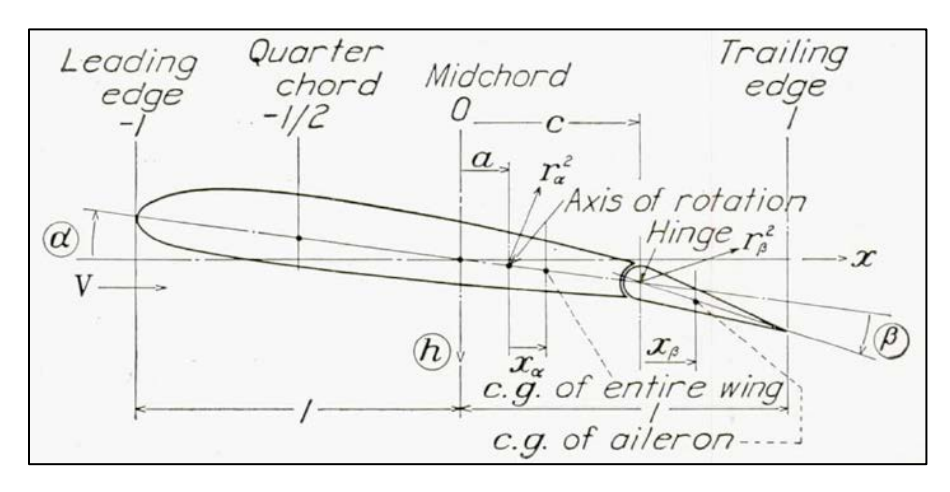
e.a. elastic axis

NACA National Advisory Committee for Aeronautics

2DOF two degree of freedom3DOF three degree of freedom

Dots over symbols denote derivatives with respect to time.

Some of the quantities in the nomenclature list and their positive senses are illustrated in the following sketch, taken from *NACA 685*:



#### 3 THEORETICAL DEVELOPMENT

The equations of motion used in the three NACA reports begin with those from reference 1 for a typical section with degrees of freedom in torsion ( $\alpha$ ), aileron deflection ( $\beta$ ), and vertical deflection (sometimes referred to as flexure) (h). These equations are three second-order differential equations in the three unknowns  $\alpha$ ,  $\beta$ , and h, and their first and second time derivatives. They are comprised of aerodynamic, inertia, and restraining terms.

$$\begin{split} (\mathbf{A}) \quad \ddot{\alpha} \bigg[ \, r_{\alpha}^{\ 2} + \kappa \left( \frac{1}{8} + a^2 \right) \bigg] + \dot{\alpha} \frac{v}{b} \, \kappa \left( \frac{1}{2} - a \right) + \alpha \frac{C_{\alpha}}{Mb^2} + \ddot{\beta} \bigg[ \, r_{\beta}^{\ 2} + (c - a) x_{\beta} - \frac{T_{7}}{\pi} \kappa - (c - a) \frac{T_{1}}{\pi} \, \kappa \bigg] + \frac{1}{\pi} \dot{\beta} \kappa \frac{v}{b} \bigg[ -2p - \left( \frac{1}{2} - a \right) T_{4} \bigg] \\ + \beta \kappa \frac{v^2}{b^2} \frac{1}{\pi} (T_4 + T_{10}) + \ddot{h} \left( x_{\alpha} - a \kappa \right) \frac{1}{b} - 2\kappa \left( a + \frac{1}{2} \right) \frac{vC(k)}{b} \bigg[ \frac{v\alpha}{b} + \frac{\dot{h}}{b} + \left( \frac{1}{2} - a \right) \dot{\alpha} + \frac{T_{10}}{\pi} \frac{v}{b} \, \beta + \frac{T_{11}}{2\pi} \dot{\beta} \bigg] = 0 \end{split}$$

$$\begin{split} \text{(B)} \quad & \ddot{\alpha} \bigg[ \, r_{\beta}^{\, 2} + (c - a) x_{\beta} - \kappa \, \frac{T_{7}}{\pi} - (c - a) \frac{T_{1}}{\pi} \kappa \, \bigg] + \dot{\alpha} \, \bigg( p - T_{1} - \frac{1}{2} T_{4} \bigg) \! \frac{v}{b} \, \frac{\kappa}{\pi} + \ddot{\beta} \bigg( \, r_{\beta}^{\, 2} - \frac{1}{\pi^{2}} \kappa T_{3} \bigg) - \frac{1}{2 \, \pi^{2}} \dot{\beta} \, T_{4} T_{11} \frac{v}{b} \, \kappa \\ & + \beta \bigg[ \frac{C_{\beta}}{M b^{2}} + \frac{1}{\pi^{2}} \frac{v^{2}}{b^{2}} \kappa (T_{5} - T_{4} T_{10}) \, \bigg] + \ddot{h} \, \bigg( x_{\beta} - \frac{1}{\pi} \kappa T_{1} \bigg) \frac{1}{b} + \frac{T_{12}}{\pi} \, \kappa \, \frac{v C(k)}{b} \bigg[ \frac{v \alpha}{b} + \frac{\dot{h}}{b} + \bigg( \frac{1}{2} - a \bigg) \, \dot{\alpha} + \frac{T_{10}}{\pi} \, v \beta + \frac{T_{11}}{2 \pi} \, \dot{\beta} \bigg] = 0 \end{split}$$

(C) 
$$\ddot{\alpha}\left(x_{\alpha} - \kappa a\right) + \dot{\alpha}\frac{v}{b}\kappa + \ddot{\beta}\left(x_{\beta} - \frac{1}{\pi}T_{1}\kappa\right) - \dot{\beta}\frac{v}{b}T_{4}\kappa\frac{1}{\pi} + \ddot{h}\left(1 + \kappa\right)\frac{1}{b} + h\frac{C_{h}}{M}\frac{1}{b} + 2\kappa\frac{vC(k)}{b}\left[\frac{v\alpha}{b} + \frac{\dot{h}}{b} + \left(\frac{1}{2} - a\right)\dot{\alpha} + \frac{T_{10}}{\pi}\frac{v}{b}\beta + \frac{T_{11}}{2\pi}\dot{\beta}\right] = 0$$

Equations (A), (B), and (C) are reproduced from reference 1. Equation (A) defines the sum of the moments about the elastic axis; equation (B), the sum of the moments about the aileron hinge; and equation (C), the sum of the forces on the entire "wing" in the vertical direction. Unsteady circulatory aerodynamics are present in the equations in the form of Theodorsen's circulation function, C(k), a complex function of reduced frequency, k, comprised of Bessel functions of the first and second kind.

*NACA 685* and *NACA 741* add to these equations structural damping, g, and a modal-coupling factor,  $\xi$ . These additions will be addressed below.

## 3.1 Assumed forms of the unknowns $\alpha$ , $\beta$ , and h

The assumed form of the unknowns in equations (A), (B), and (C) is sinusoidal:

$$\alpha = \alpha_0 e^{i(k \frac{\nu}{b} t + \varphi_0)} \tag{1a}$$

$$\beta = \beta_0 e^{i(k\frac{v}{b}t + \varphi_1)} \tag{1b}$$

$$h = h_0 e^{i(k\frac{v}{b}t + \varphi_2)} \tag{1c}$$

where  $\alpha_0$ ,  $\beta_0$ , and  $h_0$  are the (infinitesimal) amplitudes of  $\alpha$ ,  $\beta$ , and h, and  $\phi_0$ ,  $\phi_1$  and  $\phi_2$  are phase angles with respect to an unspecified reference. The first and second time derivatives of  $\alpha$ ,  $\beta$ , and h are:

$$\dot{\alpha} = ik\frac{v}{b}\alpha$$
 and  $\ddot{\alpha} = -\left(k\frac{v}{b}\right)^2\alpha$ 

$$\dot{\beta} = ik\frac{v}{b}\beta \text{ and } \ddot{\beta} = -\left(k\frac{v}{b}\right)^2\beta$$

$$\dot{h} = ik\frac{v}{b}h \text{ and } \ddot{h} = -\left(k\frac{v}{b}\right)^2h.$$

## 3.2 Substitution of assumed forms into, and normalization of, equations

Making the substitutions of equations (1a) through (1c) and their time derivatives into equations (A) through (C) transforms the latter equations from three simultaneous differential equations into three simultaneous algebraic equations with complex coefficients. The algebraic equations are then normalized by the quantity  $\kappa \left(\frac{v}{b}k\right)^2$  and by their respective exponentials and amplitudes, resulting in the equations taking the form

$$(A_{a\alpha} + \Omega_{\alpha}X)\alpha + A_{a\beta}\beta + A_{ah}h = 0 (2a)$$

$$A_{b\alpha}\alpha + (A_{b\beta} + \Omega_{\beta}X)\beta + A_{bh}h = 0$$
 (2b)

$$A_{c\alpha}\alpha + A_{c\beta}\beta + (A_{ch} + \Omega_h X)h = 0.$$
 (2c)

The quantities  $A_{\alpha\alpha}$ , etc. contain both aerodynamic and structural contributions. They are complex functions of reduced frequency, with real parts  $R_{\alpha\alpha}$ , etc. and imaginary parts  $I_{\alpha\alpha}$ , etc.

The physical parameters of the problem  $(a, b, c, \kappa, x_{\alpha}, r_{\alpha}, x_{\beta}, r_{\beta}, \omega_{\alpha}, \omega_{\beta}, \text{ and } \omega_{h})$  reside in the  $A_{ij}$  and  $\Omega_{i}X$  terms.

# 3.3 Products $\Omega_{\alpha}X$ , $\Omega_{\beta}X$ , and $\Omega_{h}X$

In equations (2a), (2b), and (2c), the products  $\Omega_{\alpha}X$ ,  $\Omega_{\beta}X$ , and  $\Omega_{h}X$  are real. They are derived from quantities  $\frac{C_{\alpha}}{Mb^{2}}$  (from eqn. (A)),  $\frac{C_{\beta}}{Mb^{2}}$  (from eqn. (B)), and  $\frac{C_{h}}{Mb}$  (from eqn. (C)), respectively. Via the substitution and rearrangement of terms and the use of cancelling expressions in the numerator and denominator, from [1] these products are

$$\Omega_{\alpha}X = \frac{C_{\alpha}}{k^2 M v^2 \kappa} = \left(\frac{\omega_{\alpha} r_{\alpha}}{\omega_r r_r}\right)^2 \frac{1}{\kappa} \left(\frac{b r_r \omega_r}{v k}\right)^2$$
(3a)

$$\Omega_{\beta}X = \frac{C_{\beta}}{k^2 M v^2 \kappa} = \left(\frac{\omega_{\beta} r_{\beta}}{\omega_r r_r}\right)^2 \frac{1}{\kappa} \left(\frac{b r_r \omega_r}{v k}\right)^2 \tag{3b}$$

$$\Omega_h X = \frac{C_h b^2}{k^2 M v^2 \kappa} = \left(\frac{\omega_h}{\omega_r r_r}\right)^2 \frac{1}{\kappa} \left(\frac{b r_r \omega_r}{v k}\right)^2 \tag{3c}$$

where, to the right of the second equal sign in each equation, X comprises the two right-most terms

$$X = \frac{1}{\kappa} \left( \frac{br_r \omega_r}{vk} \right)^2 \tag{4}$$

and the respective  $\Omega_i$ , the remaining terms

$$\Omega_{\alpha} = \left(\frac{\omega_{\alpha} r_{\alpha}}{\omega_{r} r_{r}}\right)^{2} \tag{5a}$$

$$\Omega_{\beta} = \left(\frac{\omega_{\beta} r_{\beta}}{\omega_{r} r_{r}}\right)^{2} \tag{5b}$$

$$\Omega_h = \left(\frac{\omega_h}{\omega_r r_r}\right)^2. \tag{5c}$$

The quantities  $\omega_r$  and  $r_r$  are a reference frequency and a reference length, which may be conveniently chosen.

Referring back to the normalization that produced equations (2a) through (2c), a critically important result is that the quantity X has been conveniently isolated from the other terms in these equations and it is the only quantity in these equations that contains the velocity. Therefore, solving these equations for X determines the flutter velocity,  $v_f$ . As will be seen later, X is a clever artifice created by Theodorsen: at times X is treated not as the known quantity defined in equation (4), but rather as a parameter; at other times X is treated as a known quantity.

## 3.4 Addition of structural damping, g, to the equations of motion

NACA 685 employs structural damping as "... a force in phase with the velocity but of a magnitude proportional to the restoring force." It identifies the restoring forces as the stiffness terms multiplied by their respective displacements  $(C_{\alpha}\alpha, C_{\beta}\beta, \text{ and } C_{h}h)$  in equations (A), (B), and (C).

The stiffness terms  $C_{\alpha}$ ,  $C_{\beta}$ , and  $C_h$  are also seen to reside in equations 3(a), 3(b), and 3(c). Thus, to incorporate the structural damping forces into the equations of motion merely requires that factors  $(1 + ig_{\alpha})$ ,  $(1 + ig_{\beta})$ , and  $(1 + ig_{h})$  multiply terms  $C_{\alpha}$ ,  $C_{\beta}$ , and  $C_{h}$ , respectively. Within the parentheses the "1" denotes the stiffness terms already present in the equations and the "+ig" denotes the added structural damping terms. When these factors are included, the following modified form of the equations of motion results:

$$(A_{a\alpha} + \Omega_{\alpha}(1 + ig_{\alpha})X)\alpha + A_{a\beta}\beta + A_{ah}h = 0$$
 (6a)

$$A_{b\alpha}\alpha + (A_{b\beta} + \Omega_{\beta}(1 + ig_{\beta})X)\beta + A_{bh}h = 0$$
 (6b)

$$A_{c\alpha}\alpha + A_{c\beta}\beta + (A_{ch} + \Omega_h (1 + ig_h)X)h = 0.$$
 (6c)

## 3.5 Addition of modal-coupling factor, $\xi$ , to the 2DOF form of the equations of motion

*NACA 685* devotes much of its content to examining flutter solutions for the three 2DOF subsets available from the three-dimensional equations of motion: flexure-torsion, involving h and  $\alpha$  (referred to in *NACA 496* and *NACA 685* as Case 1); aileron-flexure, involving  $\beta$  and h (Case 2); and torsion-aileron, involving  $\alpha$  and  $\beta$  (Case 3).

To the 2DOF subsets, NACA 685 introduces what it calls a "coupling factor,"  $\xi$ . (To more accurately describe its function, the present author prefers the term "modal-coupling factor.") The modal coupling factor is intended to represent the condition "... in which only a part of the total length of the (infinitely long) wing is given the second degree of freedom." One such condition is a control surface that is not full span; another is a torsion mode whose node line departs the wing surface well before the wing tip.

In NACA 685, the modal coupling factor appears as a multiplier on the upper-right off-diagonal term of the two-dimensional equations of motion, as shown in the following example using the torsion-aileron equations

$$(A_{\alpha\alpha} + \Omega_{\alpha}(1 + ig_{\alpha}) X)\alpha + \xi A_{\alpha\beta}\beta = 0$$
 (7a)

$$A_{b\alpha}\alpha + (A_{b\beta} + \Omega_{\beta}(1 + ig_{\beta})X)\beta = 0.$$
 (7b)

Equivalently, the modal coupling factor could have appeared instead as a multiplier on the lower-left off-diagonal term. The modal coupling factor takes on values from zero (no coupling) to one (full coupling).

#### **4 SOLUTION METHODS**

Each of the three NACA reports employs a different solution method, named herein Solution Methods 1, 2, and 3. Because these solution methods were all performed "by hand" engineers of the time always sought time- and effort-saving techniques and shortcuts. This was true for Theodorsen and Garrick. As will be seen below, each of the solution methods in *NACA 496*, *NACA 685*, and *NACA 741* employed these techniques and shortcuts, and as a consequence the solution methods (progressing from 1 to 2 to 3) became easier to implement.

*NACA 496* presents two solution methods: one specifically for the 2DOF problem (Solution Method 1) and another that may be used for either the 2DOF or 3DOF problems (Solution Method 2). However, *NACA 496* employs Solution Method 1 only, leaving it to *NACA 685* to employ Solution Method 2. *NACA 741* employs Solution Method 3.

The objective of each of the solution methods is to find the values of v and k that cause equations 6(a), 6(b), and 6(c) to be satisfied. Such values are identified as  $v_f$  and  $k_f$ , the flutter velocity and the flutter reduced frequency, respectively.

#### 4.1 Preliminaries

The following information applies to the solution methods and their implementation.

# 4.1.1 Clever artifices

Each solution method also employs one or more clever artifices, initially created in *NACA* 496 but also utilized in *NACA* 685 and *NACA* 741, to enable the determination of the flutter velocity,  $v_f$ , and flutter reduced frequency,  $k_f$ . At times, X and the  $\Omega$ s are treated not as the known quantities expressed in equations (4) and (5), but rather as parameters. At other times, X and the  $\Omega$ s are treated as the known quantities.

#### 4.1.2 Tables of precomputed quantities

As an aid to themselves as they solved their own example problems, as well as an aid to the readers of their reports, in *NACA 496* and *NACA 685*, Theodorsen and Garrick precomputed the various  $R_{ij}$  and  $I_{ij}$  and compiled tables of these quantities as functions of 1/k, a, and c. In addition, they also compiled tables of the real and imaginary parts of C(k) as functions of 1/k and tables of the various  $T_i$  as functions of c.

## 4.1.3 Results plotted as continuous curves

All of the numerical flutter predictions appearing in plots in [1], [2], and [3] are presented as continuous curves. Obviously, the raw form solutions in [1], [2], and [3] were performed at discrete values of 1/k and the many parametric variations were performed at discrete values of whatever the abscissa quantity happened to be, all producing discrete results. To create the final continuous curves, Theodorsen and Garrick had to first plot these discrete results, producing discrete points on a set of axes, and finally employ templates or splines (French curves) to fit continuous curves to the discrete points. Theodorsen and Garrick never reveal, for any of their plots, how many discrete points were used to produce any given continuous curve.

#### 4.2 Solution Method 1

As stated above: (1) Solution Method 1 was introduced in *NACA 496* and is applicable to only the 2DOF problem; and (2) the equations of motion in *NACA 496* include neither structural damping, g, nor the modal coupling factor,  $\xi$ . For these reasons, in the following development of Solution Method 1, the torsion-aileron subset of the 3DOF equations is chosen and is representative of all three 2DOF subsets of the 3DOF equations. Without g and  $\xi$ , equations 7(a) and 7(b) become:

$$(A_{\alpha\alpha} + \Omega_{\alpha}X)\alpha + A_{\alpha\beta}\beta = 0 (8a)$$

$$A_{b\alpha}\alpha + (A_{b\beta} + \Omega_{\beta}X)\beta = 0. (8b)$$

The solution of equations (8a) and (8b) is obtained when their determinant is zero

$$\begin{vmatrix} A_{a\alpha} + \Omega_{\alpha} X & A_{a\beta} \\ A_{b\alpha} & A_{b\beta} + \Omega_{\beta} X \end{vmatrix} = 0.$$
 (9)

When this determinant is expanded and the various  $A_{ij}$  terms are replaced with  $R_{ij} + iI_{ij}$ , the following equation, quadratic in X with complex coefficients, results:

$$\Omega_{\alpha}\Omega_{\beta}X^{2} + \left[\left(\Omega_{\alpha}R_{b\beta} + \Omega_{\beta}R_{a\alpha}\right) + i\left(\Omega_{\alpha}I_{b\beta} + \Omega_{\beta}I_{a\alpha}\right)\right]X + \left[\left(R_{a\alpha}R_{b\beta} - I_{a\alpha}I_{b\beta} - R_{a\beta}I_{b\alpha}\right) + i\left(R_{a\alpha}I_{b\beta} + R_{b\beta}I_{a\alpha} - R_{a\beta}I_{b\alpha} - I_{a\beta}R_{b\alpha}\right)\right] = 0.$$

$$(10)$$

This solution method employs the computational shortcut of separating equation (10) into its real and imaginary components, thereby eliminating the need for complex arithmetic:

$$\Omega_{\alpha}\Omega_{\beta}X^{2} + \left(\Omega_{\alpha}R_{b\beta} + \Omega_{\beta}R_{a\alpha}\right)X + \left(R_{a\alpha}R_{b\beta} - I_{a\alpha}I_{b\beta} - R_{a\beta}R_{b\alpha} + I_{a\beta}I_{b\alpha}\right) = 0 \tag{11a}$$

$$\left(\Omega_{\alpha}I_{b\beta} + \Omega_{\beta}I_{a\alpha}\right)X + \left(R_{a\alpha}I_{b\beta} + R_{b\beta}I_{a\alpha} - R_{a\beta}I_{b\alpha} - I_{a\beta}R_{b\alpha}\right) = 0 \tag{11b}$$

where equation (11a) (from the real components of eqn. (10)) has real coefficients and is quadratic in X and equation (11b) (imaginary components) also has real coefficients and is linear in X. This separation will be referred to as the "complex-to-real computational shortcut."

At this point, the reference quantities,  $\omega_r$  and  $r_r$  are defined to be  $\omega_\beta$  and  $r_\beta$ , respectively. When  $\omega_\beta$  and  $r_\beta$  are substituted into equations (5a) and (5b),  $\Omega_\alpha$  and  $\Omega_\beta$  become

$$\Omega_{\alpha} = \left(\frac{\omega_{\alpha} r_{\alpha}}{\omega_{\beta} r_{\beta}}\right)^{2}$$

$$\Omega_{\beta} = \left(\frac{\omega_{\beta} r_{\beta}}{\omega_{\beta} r_{\beta}}\right)^2 = 1.$$

The quantity  $\Omega_{\beta}$  has been conveniently set to be unity and is thus effectively removed from equations (11a) and (11b).

The solution method now employs the artifice that quantities X and  $\Omega_{\alpha}$  are treated as parameters, rather than as the known quantities as expressed in equations (4) and (5a). Equations (11a) and (11b) are regarded as two simultaneous equations in the two unknowns X and  $\Omega_{\alpha}$  and are solved conventionally by substitution.

To begin, equation (11b) is solved for X, yielding

$$X = -\frac{R_{a\alpha}I_{b\beta} + R_{b\beta}I_{a\alpha} - R_{a\beta}I_{b\alpha} - I_{a\beta}R_{b\alpha}}{\Omega_{\alpha}I_{b\beta} + I_{a\alpha}}.$$
 (12)

This expression is then substituted into equation (11a), thereby eliminating X from that equation and producing, after several steps, the following equation, quadratic in  $\Omega_a$ :

$$\Omega_{\alpha}^{2} \left( M^{R} I_{b\beta}^{2} - M^{I} R_{b\beta} I_{b\beta} \right) + \Omega_{\alpha} \left[ -M^{I} \left( R_{\alpha\beta} I_{b\alpha} + I_{\alpha\beta} R_{b\alpha} \right) + 2 M^{R} I_{\alpha\alpha} I_{b\beta} \right] + M^{R} I_{\alpha\alpha}^{2} - M^{I} R_{\alpha\alpha} I_{\alpha\alpha} = 0$$

$$(13)$$

where the quantities  $M^R$  and  $M^I$  are shorthand notations for the constant terms in equations (11a) and (11b), respectively:

$$M^{R} = R_{a\alpha}R_{b\beta} - I_{a\alpha}I_{b\beta} - R_{a\beta}R_{b\alpha} + I_{a\beta}I_{b\alpha}$$
  
$$M^{I} = R_{a\alpha}I_{b\beta} + R_{b\beta}I_{a\alpha} - R_{a\beta}I_{b\alpha} - I_{a\beta}R_{b\alpha}.$$

With the artifice still in place, the next step in Solution Method 1 is to solve equation (13) for its two roots,  $\Omega_{\alpha_1}$  and  $\Omega_{\alpha_2}$ , for a large number of reduced frequencies. But, recalling from equation (5a) that  $\Omega_a$  is defined as the square of a quantity, only the real positive values of  $\Omega_{\alpha_1}$  and  $\Omega_{\alpha_2}$  are valid solutions of equation (13). These valid solutions are then plotted as functions of the inverse of reduced frequency, 1/k.

Next, values of X are computed by executing equation (12) for the same reduced frequencies that produced  $\Omega_{\alpha_1}$  and  $\Omega_{\alpha_2}$ . For each of these executions, the values of the constituent quantities of equation (12) (the  $R_{ij}$ s, the  $I_{ij}$ s,  $\Omega_{\alpha_1}$ , and  $\Omega_{\alpha_2}$ ) must be those at corresponding values of reduced frequency. *NACA 496* chooses to present the resulting Xs as functions of  $\Omega_a$  rather than as functions of 1/k.

At this point, a new quantity, F, the nondimensional flutter factor, is introduced

$$F = \frac{1}{k} \frac{1}{\sqrt{X}}. (14)$$

F is also treated as a parameter. The Xs and their corresponding reduced frequencies are substituted into equation (14), producing a plot of F as a function of  $\Omega_a$ , again containing both  $\Omega_{\alpha_1}$  and  $\Omega_{\alpha_2}$ .

The two curves,  $\Omega_a$  vs. 1/k, and F vs.  $\Omega_a$ , represent a family of flutter solutions over a range of  $\Omega_a$ . Each point on the first curve has a corresponding point on the second and each pair of corresponding points represents a unique flutter solution.

To obtain a specific flutter solution from the family of solutions, the artifice is abandoned: quantities  $\Omega_a$ , X, and F are no longer interpreted as parameters and equations (5a) and (4) are employed. In addition, when the expression in equation (4) is substituted for X in equation (14), the flutter factor becomes

$$F = \frac{\sqrt{\kappa v}}{b\omega_r r_r}. (15)$$

When solved for flutter velocity, equation (15) becomes

$$v_f = F \frac{b\omega_r r_r}{\sqrt{\kappa}}. (16)$$

Thus, once a family of flutter solutions is obtained, the following simple two-step process for obtaining a specific flutter solution from the family of solutions may be performed:

Identify flutter reduced frequency. – Problem-specific values of  $\omega_{\alpha}$ ,  $r_{\alpha}$ ,  $\omega_{r}$ , and  $r_{r}$  are substituted into equation (5a), yielding a problem-specific value of  $\Omega_{\alpha}$ . This value of  $\Omega_{\alpha}$  is located in the plot of  $\Omega_{\alpha}$  vs. 1/k. The value of 1/k corresponding to this value of  $\Omega_{\alpha}$  then yields, via its inverse, the flutter reduced frequency,  $k_{f}$ .

Identify flutter velocity. – The problem-specific value of  $\Omega_{\alpha}$  is located in the plot of F vs.  $\Omega_{\alpha}$ . The value of F corresponding to this value of  $\Omega_{\alpha}$  and problem-specific values of E, E, E, and E are substituted into equation (16), yielding the flutter velocity, E,

Figure 1 is an example of the pair of plots created in Solution Method 1 and correspond to Case 3, torsion-aileron. The plots are figures 5 and 6, scanned from *NACA 496*. The dashed colored lines in the plot of  $\Omega_{\alpha}$  vs. 1/k illustrate the determination of flutter reduced frequency from the problem-specific value of  $\Omega_{\alpha}$ . The dashed colored lines in the plot of F vs.  $\Omega_{\alpha}$  illustrate the determination of flutter velocity, also from the problem-specific value of  $\Omega_{\alpha}$ .

## 4.3 Solution Method 2

As stated above: (1) Solution Method 2 is applicable to either the 2DOF problem or the 3DOF problem and is implemented in *NACA 685*; and (2) structural damping, g, and the modal coupling factor,  $\xi$ , may each be present. This solution method differs from Solution Method 1 in that the

 $\Omega$ s are not treated as parameters; they are treated as known quantities expressed in equations (3a), (3b), and (3c). In the Summary of *NACA 685*, the authors say "... the basic flutter theory [is] ... simpler ..." than the one in *NACA 496*. Indeed it is.

Addressing first the 3DOF problem, equations (6a), (6b), and (6c) are employed. The solution of these equations is obtained when their determinant is zero:

$$\begin{vmatrix} A_{a\alpha} + \Omega_{\alpha}(1+ig_{\alpha})X & A_{a\beta} & A_{ah} \\ A_{b\alpha} & A_{b\beta} + \Omega_{\beta}(1+ig_{\beta})X & A_{bh} \\ A_{c\alpha} & A_{c\beta} & A_{ch} + \Omega_{h}(1+ig_{h})X \end{vmatrix} = 0.$$
 (17)

Expanding the determinant in equation (17) yields a complex cubic equation in X.

Rather than solving directly this complex cubic equation, *NACA 685* also employs the complex-to-real computational shortcut, resulting in two equations with real coefficients. To distinguish the origins of these equations one will be referred to as the "real equation" and the other, the "imaginary equation." Because of the presence of structural damping, both the real and imaginary equations are cubic in *X* with real coefficients. If structural damping is not present, the real equation is still cubic but the imaginary equation becomes quadratic. In the interest of space, these equations are omitted.

Addressing next the 2DOF problem, using equations (7a) and (7b) as the example, the solution is obtained when their determinant is zero

$$\begin{vmatrix} A_{a\alpha} + \Omega_{\alpha}(1 + ig_{\alpha}) X & \xi A_{a\beta} \\ A_{b\alpha} & A_{b\beta} + \Omega_{h\beta} (1 + ig_{\beta}) X \end{vmatrix} = 0.$$
 (18)

Expanding the determinant in equation (18) yields a complex quadratic equation in X.

Again employing the complex-to-real computational shortcut, real and imaginary equations result that are quadratic in *X* with real coefficients. If structural damping is not present, the real equation is still quadratic but the imaginary equation becomes linear. In the interest of space, these equations are also omitted.

Solution Method 2 is a straightforward four-step process aimed at finding the flutter velocity,  $v_f$ , and the flutter reduced frequency,  $k_f$ , that simultaneously solve both the real and imaginary equations, and therefore, also solves the original equation with complex coefficients:

Solve real and imaginary equations for X. – The artifice of treating X as a parameter, rather than as a known quantity, is employed. The real and imaginary equations are each solved for X for many values of the inverse of reduced frequency, 1/k. The Xs from the real equation and the Xs from the imaginary equation are then plotted on the same set of axes as functions of 1/k, with each equation producing the same number of loci as the order of the respective equation. (These loci are not what are

commonly referred to as classical root loci.) Each point of each real locus is a solution of the real equation; each point of each imaginary locus is a solution of the imaginary equation.

Identify intersections of real and imaginary loci. – Intersections of any of the real loci with any of the imaginary loci are simultaneous solutions of both equations, and therefore, are also solutions of the original equation with complex coefficients, thus supplying pairs of values, X and 1/k, that satisfy the original equation. However, these pairs of X and 1/k are not necessarily flutter solutions. Because, X is proportional to the inverse square of velocity (eqn. (4)), only those intersections of the loci involving real positive values of X (and therefore real – not complex or imaginary – velocities) are flutter solutions. These intersections will be termed "proper" intersections and the corresponding pairs of X and 1/k will be termed "proper" pairs. After all proper intersections and pairs have been determined, the artifice of treating X as a parameter is abandoned. (The term "proper" in this context is an invention of the present author and is not found in NACA 685.)

<u>Identify flutter reduced frequency</u>. – From each proper pair, its flutter reduced frequency,  $k_f$ , is determined from the inverse of 1/k.

<u>Identify flutter velocity</u>. – From each proper pair, its flutter velocity is determined by rearranging equation (4) to solve for velocity

$$v_f = \frac{1}{\sqrt{\kappa}} \frac{b\omega_r r_r}{k_f} \frac{1}{\sqrt{X}}.$$
 (19)

The value of  $k_f$  from the step above, its corresponding value of X, and the problem-specific quantities  $\kappa$ , b,  $r_r$ , and  $\omega_r$  are substituted into equation (19), yielding the flutter velocity. Multiple proper intersections and pairs indicate multiple flutter solutions.

Figure 2 is an example illustration of Solution Method 2 for the 3DOF case. The plot is a scanned image of figure 4 from *NACA 685* and corresponds to a single flutter mode. The intersection of a real locus with an imaginary locus identifies the flutter condition, with flutter reduced frequency and flutter velocity determined as shown by the dashed colored lines in the figure.

# 4.4 Solution Method 3

Solution Method 3 is applicable to either the 2DOF problem or the 3DOF problem and is implemented in *NACA 741*. Structural damping, g, and the modal coupling factor,  $\xi$ , may each be present.

The starting point for this solution method is the real and imaginary equations described in connection with Solution Method 2 that result from the complex-to-real computational shortcut. As was seen above, depending on the number of degrees of freedom present and the presence or absence of structural damping, the real equation can be either cubic or quadratic and the imaginary equation can be cubic, quadratic, or linear.

Next, employing a method analogous to Sylvester's method of elimination [9], the real and imaginary equations are transformed from their original orders in X to linear equations in X in the forms

$$a_1 X + a_0 = 0 (20)$$

$$b_1 X + b_0 = 0 (21)$$

where the X in equation (20) becomes identified as  $X_1$  and the X in equation (21), as  $X_2$ . The coefficients  $a_0$ ,  $a_1$ ,  $b_0$ , and  $b_1$  are intricate combinations of the coefficients of the real and imaginary equations that result from the method of elimination. While it was a time-consuming task to obtain the coefficients in equations (20) and (21), once they were obtained it was a trivial task to solve these equations for X.

At this point Solution Method 3 follows a four-step process analogous to that of Solution Method 2:

Solve equations (20) and (21) for X. – The artifice of treating X as a parameter, rather than as a known quantity, is employed. Equations (20) and (21) are each solved for X for many values of the inverse of reduced frequency, 1/k. Quantities  $X_1$  and  $X_2$  are then plotted on the same set of axes as functions of 1/k.

Identify intersections of equations (20) and (21). – Intersections of  $X_1$  and  $X_2$  are simultaneous solutions of both equations, and therefore, are also solutions of the original equation with complex coefficients, thus supplying pairs of values, X and 1/k, that satisfy the original equation. However, as with Solution Method 2, the same restriction on real positive values of X applies and the resulting pairs of X and 1/k are also termed proper pairs.

<u>Identify flutter reduced frequency</u>. – From each proper pair, its flutter reduced frequency,  $k_f$ , is determined from the inverse of 1/k.

<u>Identify flutter velocity</u>. – From each proper pair, its flutter velocity is determined by applying equation (19).

Figure 3 is an example illustrating Solution Method 3 for the 3DOF case and corresponds to a single flutter mode. NACA~741 does not contain any figures that illustrate the raw form of Solution Method 3, that is, it does not contain any figures that resemble, figure 3. NACA~741 contains only plots of nondimensional flutter speed as functions of various quantities. In figure 3 the intersection of  $X_1$  and  $X_2$  identifies the flutter condition, with flutter reduced frequency and flutter velocity determined as shown by the dashed colored lines in the figure. (As will be seen later in this paper, in actual practice Solution Method 3 can produce values of  $X_1$  and  $X_2$  that range over several orders of magnitude. Additionally, values of 1/k necessary to capture all the proper intersections of a given problem can also range over several orders of magnitude. For these reasons, it was found that log-log plots are the best way to visualize the behaviors of  $X_1$  and  $X_2$  with increasing values of 1/k.)

#### **5 TRIPPING POINTS**

As used in this paper, the term "tripping point" is an aspect of references 1, 2, or 3 that has the potential to cause confusion. Unfortunately, the present author discovered, via tripping, several tripping points, especially in *NACA 496*. Some are fairly innocuous; others, less so. Listed here are a few of the "less so" tripping points.

#### 5.1 Tripping point no. 1

NACA 496 contains in its main text and in its Appendix I ("Procedure in Solving Numerical Examples") equations for the various  $I_{ij}$ . In the main text each equation for  $I_{ij}$  contains the multiplying factor 1/k; those in Appendix I do not. The author of NACA 496 obscures this difference by giving both sets of equations the same equation numbers and by alerting the reader to this difference in footnote form only, rather than in a more direct way. Compounding this obscuring is the fact that the author of NACA 496 gave no explanation for the difference. For the present author, all of these things became "part A" of this tripping point.

The reason for the missing factor in Appendix I, never stated in *NACA 496*, was to avoid unnecessary calculations when engineers of the time solved a numerical example according to the procedure outlined in Appendix I. Equation (11b) illustrates how the unnecessary calculations were avoided. The left-hand side of any equation whose right-hand side is zero, may be multiplied or divided by any factor without altering the solution of that equation. Equation (11b) satisfies this condition because each term in the equation is a product containing an  $I_{ij}$ . Thus, depending on which form of the  $I_{ij}$  is chosen, the entire equation either does or does not contain the factor 1/k. So, regardless of the factor's presence or absence, the solution of equation (11b) will be the same. Therefore, to avoid the unnecessary multiplications by 1/k in obtaining the terms in equation (11b), the author of *NACA 496* omitted them.

However, omitting the factor has a consequence on equation (11a), which the author of *NACA 496* failed to point out, and represented "part B" of the tripping point for the present author. When the factor 1/k is removed from the  $I_{ij}$ , equation (11a) must be modified to "reinstall" the multiplying factor  $1/k^2$  in two of its products:  $I_{a\alpha}I_{b\beta}$  and  $I_{a\beta}I_{b\alpha}$ .

When combined, parts A and B represented a significant tripping point for the present author, who initially missed the footnote, failed to notice the difference in the expressions for  $I_{ij}$  in the main text and Appendix I, and did not immediately recognize the consequence on equation (11a) of removing the factor 1/k.

#### 5.2 Tripping point no. 2

NACA 496 contains a second tripping point similar to the first. The nine expressions for  $R_{ij}$  and the nine for  $I_{ij}$  are derived from equations (A), (B), and (C). In rederiving these expressions the present author duplicated 12 of the 18 expressions. The six expressions not duplicated were the three expressions for  $R_{ij}$  and the three for  $I_{ij}$  that make up the entirety of equation (C). The expressions published in NACA 496 each lacked a factor of 1/b compared to what the present author found.

As it turns out, the missing 1/b factors are of no consequence in these expressions for the same reason that the missing 1/k factors were of no consequence above: The left-hand side of any equation whose right-hand side is zero, may be multiplied or divided by any factor without altering the solution of that equation. And omitting the 1/b factor was done for the same reason: to avoid the unnecessary multiplications by 1/b in obtaining the terms in equation (C).

## 5.3 Tripping point no. 3

A third tripping point in NACA 496 involves the nondimensional flutter factor, F, defined in NACA 496 (and eq. (14), herein) as

$$F = \frac{1}{k} \frac{1}{\sqrt{X}}$$
.

The author of *NACA 496* states that sometimes the quantity  $\frac{1}{k^2}\frac{1}{X}$  is used in the plots for Solution Method 1 and sometimes the quantity  $\frac{1}{k}\frac{1}{\sqrt{X}}$  is used. Not directly articulated by the author, but certainly understood by the reader, is that sometimes the quantity  $F^2$  is used in the plots and sometimes the quantity F is used. However, in the plots in *NACA 496*, the same symbol, F, is used in both instances! This double use of a symbol to represent not only its original definition, but also the square of its original definition, represented a significant tripping point for the present author when trying to reproduce figures 6, 8, and 10 in *NACA 496*.

## 6 COMPARISON OF ORIGINAL AND RECOMPUTED RESULTS

As stated earlier, a purpose of the present paper is to report on a multiyear effort to recompute all of the numerical examples predicting flutter in references 1, 2, and 3. For each of these NACA reports the recomputations were performed using the solution method specific to that report and spot-checked using an independent solution method. To date, recomputations have been completed for references 1 and 2 and have begun for reference 3.

### **6.1 Preliminaries**

The following information applies to the comparisons shown in this paper of the original and recomputed results.

#### 6.1.1 Down-selection of comparisons

If one includes in the count all the parameter variations, there are more than four hundred separate plots containing computed flutter results in [1], [2], and [3]. To include hundreds of comparisons is beyond the scope of the present paper. Therefore, a significant down-selection had to be made. The criteria for a comparison surviving this down-selection are the following:

The comparison is an example of a solution method in its "raw" form;

The comparison is representative of the quality of similar comparisons;

The comparison illustrates an error or tripping in the original results.

# 6.1.2 Unknown number of discrete values of quantities required to produce original plots

Recall that all of the numerical flutter predictions appearing in plots in references 1, 2, and 3 are presented as continuous curves. Theodorsen and Garrick never reveal in these references the number of discrete values of 1/k required to produce a raw flutter solution nor do they ever reveal the number of raw solutions required to produce any of the parametric variations. Because of the significant effort required at the time to obtain even a single flutter solution "by hand," one would assume these numbers were "as few as possible," giving rise to the possibility (probability?) that the resulting continuous curves were based to some degree on engineering judgement (how many and which values of 1/k to use?, how many and which raw flutter solutions to use?, which French curve to use to fair through the points?). As will be seen in instances below, "as few as possible" would explain why, for many of the parametric variations, the original curves are characterized by less abrupt changes in slope than are the recomputed curves – they were faired using fewer points.

# 6.1.3 Numerical checks of the recomputed results

Recomputed results were spot-checked.

The numerical checks for *NACA 496* were performed by a colleague of the present author who implemented in Matlab® the equations found in reference 5 for a typical section, including unsteady aerodynamics defined by the Theodorsen circulation function. The code loops on velocity. For each velocity, the calculations are run through an iterative loop until the frequencies are converged, followed by an evaluation of damping values to determine if the system is stable or unstable

The numerical checks for NACA 685 and NACA 741 were performed by the present author using the p-method of flutter solution [10]. The advantage of the p-method is that it produces a classical velocity root locus in the Laplace domain. In circumstances where the NACA 685 and NACA 741 solution methods produced multiple flutter conditions (i.e., multiple proper intersections), the p-method was ideal for determining the nature of those flutter conditions – for example, whether there were two separate flutter modes, each of which went unstable and remained unstable with increasing velocity, or whether the intersections corresponded to a "hump mode" that went unstable at one velocity but then restabilized at a higher velocity.

The *p*-method was written and coded in Matlab® by the present author following the formulation outlined in Appendix B of reference 11. This implementation of the *p*-method employs a fourth-order-over-fourth-order approximation of Theodorsen's circulation function, C(k), identified in reference 12 as the "balanced truncation" approximation. This approximation is excellent: over the range of reduced frequency 0.001 < k < 10 it approximates to within 0.2 percent the complex modulus of C(k) and approximates to within 0.25 degrees the phase angle of C(k).

In almost all instances, the spot-checked answers (flutter velocity and flutter reduced frequency) were within 0.5 percent of the recomputed results (no difference exceeded 2 percent), giving confidence that the recomputed results presented herein are correct.

## 6.1.4 Presentation of original and recomputed results

Figures and graphs from [1], [2], and [3] have been electronically scanned and are included in the present paper. Recomputed results have been superimposed on these originals and keys have been added to each figure and graph.

The manner of distinguishing between the original and recomputed results is through the use of color according to the following conventions:

For figures with no parameter variations, the original results are black curves and the recomputed results are either colored symbols or colored curves.

For figures with parameter variations, the original results are black curves overlaid with color bands specific to a particular value of the parameter and the recomputed results are symbols of the corresponding color.

## 6.2 Comparisons of original and recomputed results for NACA 496

Three comparisons were chosen for *NACA 496*. The first illustrates the raw form of Solution Method 1; the second illustrates an error in *NACA 496*; and the third illustrates a tripping point.

# 6.2.1 Comparison no. 1

Figure 4 contains comparisons for figs. 9 and 10 of *NACA 496* and illustrates Solution Method 1 for Case 1, flexure-torsion. Figure 4(a) shows the plot of  $\Omega_h$  vs. 1/k and 4(b) shows the plot of F vs.  $\Omega_h$ .

While there are some differences between the original and recomputed results, the overall magnitudes and shapes of the respective curves are very similar. In figure 4(a), the original curve does not "touch" the vertical axis, whereas the recomputed curve does. This trend is repeated in figure 4(b), but for the horizontal axis.

Tripping point no. 3, described above, is present in figure 4(b). Although the ordinate in this figure is labelled "F", the quantities plotted (original and recomputed) are actually  $F^2$ .

## 6.2.2 Comparison no. 2

Figure 5 contains comparisons for fig. 14 of *NACA 496* and illustrates an error in *NACA 496*. This example is for curve A and is, again, for Case 1, flexure-torsion. Flutter factor (as defined) is presented as a function of the nondimensional distance from the elastic axis to the center of gravity.

The solid colored circles in figure 5 were obtained by executing Solution Method 1 six times, with a different value of  $x_{\alpha}$  employed in each solution, resulting in six standard pairs of curves. Next, for each pair of curves, a specific value of frequency ratio (in this case,  $\omega_1/\omega_2 = 1/6$ ) was used to determine the specific value of  $\Omega_h$ , from which the corresponding specific value of F was obtained. These values of F were plotted as a function of  $x_{\alpha}$ , resulting in the colored circles.

As a check on the recomputed results, independent calculations were performed by a colleague. The numerical checks are indicated by the white X symbols.

It is seen that curve A and the recomputed results show opposite trends with increasing values of  $x_{\alpha}$ . However, the present author observed the following: the recomputed value of F at  $x_{\alpha} = 0$  is very close to the original value of F at  $x_{\alpha} = 0.4$  and vice versa; the recomputed value of F at  $x_{\alpha} = 0.1$  is very close to the original value of F at  $x_{\alpha} = 0.3$  and vice versa; and the recomputed value of F at  $x_{\alpha} = 0.2$  is very close to the original value of F at  $x_{\alpha} = 0.2$ . This observation led to the rotation of original curve A about the vertical axis  $x_{\alpha} = 0.2$ .

The rotated curve A, the colored circles, and the white X symbols exhibit excellent agreement with each other. This triple agreement suggested to the present author that original curve A was incorrectly plotted. (Although not presented in this figure, the results for curves B and C also show triple agreements after original curves B and C are similarly rotated.)

In the early 1930s, intricate and multistepped engineering calculations, such as those required to produce the results in *NACA 496*, were performed by hand; results were recorded and transcribed by hand; and then plotted by hand. It is not unrealistic to expect that, with the many steps performed by humans, errors occurred. The present author believes, that in the case of figure 5, transcription errors occurred – correct values of F were paired with noncorresponding values of  $x_{\alpha}$  – which then led to an incorrect plot.

## 6.2.3 Comparison no. 3

Figure 6 contains comparisons for fig. 16 of NACA 496 and illustrates a tripping point in NACA 496.

The curves in figure 6 are plots of flutter velocity as a function of frequency ratio for the Case 2, the aileron-flexure subset. To obtain these curves, first the aileron-flexure solution method was executed, resulting in a curve of F (this time, as defined) vs.  $\Omega_{\beta}$ . Next, flutter velocity was obtained from F by employing equation (16). Finally, on the abscissa, the frequency ratio,  $\omega_{\beta}/\omega_{h}$ , was obtained from  $\Omega_{\beta}$  by employing equation (5b).

From equations (16) and (5b), respectively, to obtain the dimensional flutter velocity and the frequency ratio, values of reference quantities  $\omega_r$  and  $r_r$  are required. For the aileron-flexure subset,  $\omega_r$  and  $r_r$  are  $\omega_h$  and 1, respectively. But, in another tripping point, NACA 496 does not supply the value of  $\omega_h$  it used in the creation of this figure. Therefore, for the recomputed calculations, a value of  $\omega_h$  had to be assumed. Via trial and error, the value chosen ( $\omega_h = 5.8 \text{x} 2\pi$ ) was the one that produced the best agreement (based on trying to match the highest values of  $\omega_{\beta}/\omega_h$  for which flutter occurred) between the recomputed curves and the originals.

There are noticeable differences between the original and recomputed results in figure 6, in places on the order of 35%, but the overall magnitudes and shapes of the respective curves are similar.

NACA 496 contains in two of its original figures, its fig. 8 (not shown in the present paper) and its fig. 16 (shown in the present paper as figure 6), predictions of hump-mode flutter – each prediction with a range of frequency ratios over which there are a lower and an upper solution to the equations for any given value of the frequency ratio. These predictions of hump-mode flutter may be the first in the field of aeroelasticity!

## 6.3 Comparisons of original and recomputed results for NACA 685

NACA 685 presents its results in two different forms: "figures" and "graphs." The figures are uncluttered and straightforward, and may contain either 2DOF or 3DOF results; graphs are packed with parameter variations and multiple parts and contain 2DOF results only.

In NACA 685, all graphs with Roman numeral "I" contain predictions of flutter for Case 1, flexure-torsion; graphs with "II", Case 2, aileron-flexure; graphs with "III", Case 3, torsion-aileron.

Four comparisons were chosen for *NACA 685*. The first illustrates the raw form of Solution Method 1; the second illustrates a set of parameter variations; the third and fourth illustrate errors in *NACA 685*.

# 6.3.1 Comparison no. 4

Figure 7 contains comparisons for fig. 7(c) of *NACA 685* and illustrates a raw result for Solution Method 2 for the 3DOF flutter problem. The reproduction of fig. 7(c) has been enlarged for the purpose of clarity.

With one exception (the original and recomputed imaginary loci at the bottom right of the figure), the original and recomputed loci in figure 7 show good-to-excellent agreement. There are three proper intersections of real and imaginary loci, predicted both in the original and recomputed results and highlighted by the dashed circles. Visually, the agreement between the values of  $\sqrt{X}$  and 1/k at the original and recomputed intersections is excellent. As confirmed by a numerical check using the p-method of flutter solution, these intersections correspond to a classical flutter mode (bottom-most intersection) and a hump mode (two top-most intersections).

## 6.3.2 Comparison no. 5

Figure 8 is a representative example of the quality of agreement among many of the parametric variations in *NACA 685*.

Graph I-A contains 21 parts and shows the effect of increasing values of frequency ratio,  $\frac{\omega_h}{\omega_{\alpha'}}$  on nondimensional flutter speed,  $\frac{v_f}{b\omega_{\alpha'}}$ , with  $x_{\alpha}$ , the distance between the elastic axis and the center of gravity of the entire wing, as the parameter. The various parts of this graph cover ranges of mass ratios,  $\kappa$ , and non-dimensional distance from midchord to the elastic axis, a.

Figure 8 contains eight of these 21 parts and corresponds to parts "j" through "q" of Graph I-A. The agreement between the original and recomputed results ranges from excellent in some places to poor in others. In all parts of the graph (that is, over the entire ranges of  $\kappa$  and  $\alpha$  and for all values of  $\kappa$ , up to values of  $\kappa$  of about 0.8, there is good-to-excellent agreement between the original and recomputed results. In the parts of the graph shown in figure 8 (as well as other parts not shown here), the mutual crossings of the red, blue, and green curves (original results) and the mutual crossing of the red, blue, and green symbols (recomputed results) are in excellent agreement.

Above values of  $\frac{\omega_h}{\omega_\alpha}$  of about 0.8, some of the curves continue to display good-to-excellent agreement, but in many instances the original and recomputed results differ significantly. One common difference between the original and recomputed results is illustrated by the blue results  $(x_\alpha=0.2)$  in part (l) and the red results  $(x_\alpha=0.1)$  in part (n): with increasing values of  $\frac{\omega_h}{\omega_\alpha}$  both sets of results reach a minimum and then increase, but in the vicinity of their respective minima the recomputed results display much steeper slopes (negative and positive) than do the original results. Another common difference between the original and recomputed results is illustrated by the blue results  $(x_\alpha=0.2)$  in part (j) and the red results  $(x_\alpha=0.1)$  in part (l): with increasing values of  $\frac{\omega_h}{\omega_\alpha}$  the original results reach a minimum and then increase, but (at least over the range of  $\frac{\omega_h}{\omega_\alpha}$  shown) the recomputed results continue to decrease.

# 6.3.3 Comparison no. 6

Figure 9 corresponds to Graph I-G of *NACA 685* and shows the effect of increasing values of frequency ratio,  $\frac{\omega_h}{\omega_\alpha}$ , on nondimensional flutter speed,  $\frac{v_f}{b\omega_\alpha}$ , with the modal coupling factor,  $\xi$ , as the parameter. For modal coupling factor of unity, the character of the original and recomputed results is the same, with excellent agreement at low values of frequency ratio but with about a 30% difference at the highest value. For coupling factors less than unity, the characters of the original and recomputed results differ significantly: the original results show hump modes for only small ranges of frequency ratio; recomputed results show hump modes over the entire ranges of instability. For the lower values of nondimensional flutter speed, the original and recomputed results show excellent agreement up to frequency ratios of 0.7, 0.8, and 1.0 for modal coupling factors of  $\frac{3}{8}$ ,  $\frac{1}{2}$ , and  $\frac{3}{4}$ , respectively.

# 6.3.4 Comparison no. 7

Figure 10 corresponds to Graph II-A of *NACA 685* and shows the effect of increasing values of frequency ratio,  $\frac{\omega_{\beta}}{\omega_{h}}$ , on nondimensional flutter speed,  $\frac{v_{f}}{b\omega_{h}}$ , for three different parameter variations: parts (a) and (b) have  $x_{\beta}$  as the parameter; part (c) has  $g_{\beta}$  and  $g_{h}$  as parameters; and part (d) has  $r_{\beta}^{2}$  as the parameter. For all parts of the graph b=6,  $c=\frac{1}{2}$ ,  $\omega_{h}=22.5$ , and  $\xi=1$ . Discrete values and ranges of values of the other physical constants are indicated in the legend for each part of the graph.

In all parts of the graph, the original results and the recomputed results indicate hump modes over the ranges of the independent variable. And, except for part (b), the original and recomputed results show good-to-excellent agreement. Part (b) shows significant disagreement between the magnitudes of nondimensional flutter speeds, especially for  $x_{\beta} = \frac{1}{30}$ . The disagreements for part (b) are addressed in the next paragraph.

Part (b) presents results for parametric variations in  $x_{\beta}$  for a constant value of  $r_{\beta}^2$ ; part (d) presents results for parametric variations in  $r_{\beta}^2$  for a constant value of  $x_{\beta}$ . All other physical constants are

identical for parts (b) and (d) (b = 6,  $c = \frac{1}{2}$ ,  $\kappa = \frac{1}{10}$ ,  $\omega_h = 22.5$ ,  $g_\beta = 0$ ,  $g_h = 0$ , and  $\xi = 1$ ). One set of results in part (b) shares identical physical constants with a set of results in part (d) ( $x_\beta = \frac{1}{60}$  and  $r_\beta^2 = \frac{1}{120}$ , ) and coincidentally, both sets are represented in their respective parts by red curves and symbols. Therefore, one would expect that the original results in parts (b) and (d) would be identical to each other as would the corresponding recomputed results. This is the case for the recomputed results (the red symbols in each part have identical values at corresponding values of frequency ratio), but this is not the case for the original results (the red curves display noticeably different values). This difference in original values between parts (b) and (d), coupled with the good-to-excellent agreement between the original and recomputed in all other parts of the graph and successful checks of the recomputed results using the *p*-method of flutter solution, strongly suggests that all original results in part (b) are in error.

# 6.4 Comparisons of original and recomputed results for NACA 741

As its title states, *NACA 741* contains flutter results for three degrees of freedom only. The present work of comparing original and recomputed results for *NACA 741* has recently begun. To date, only one comparison among the five potential comparisons in fig. 1 of *NACA 741* has been completed. This comparison is shown in figure 11 and illustrates an omission in *NACA 741*.

# 6.4.1 Comparison no. 8

Figure 11(a) shows the effect of increasing values of frequency ratio,  $\frac{\omega_{\beta}}{\omega_{\alpha}}$ , on nondimensional flutter speed,  $\frac{v_f}{b\omega_{\alpha}}$ , for several positive and negative values of  $x_{\beta}$ , the nondimensional distance from the aileron hinge to the center of gravity (c.g.) of the aileron. The one comparison within figure 11(a) is for  $x_{\beta}=0.004$ , indicating that the c.g. is aft of the hinge line. NACA 741 predicts a single flutter mode, indicated by the black line with the red color band. The recomputed results are indicated by the solid red circles and are in very close agreement with the original results over most of the range of frequency ratio. However, as has been seen in other comparisons, and probably due to a coarse spacing of frequency ratio, the original results missed the steep dip and subsequent steep rise in nondimensional flutter speed near the recomputed minimum non-dimensional flutter speed at  $\frac{\omega_{\beta}}{\omega_{\alpha}}=0.5$ .

Figure 11(b) is an enlargement of the lower-left corner of figure 11(a). The red color band and red solid circles from figure 11(a) have been muted in order to not distract from the blue solid circles. The blue solid circles are also recomputations and indicate the presence of a hump mode, which was not predicted by Theodorsen and Garrick. The hump mode was also predicted by the present author by employing the p-method and by a colleague of the present author by employing both a different implementation of the p-method and the k-method. These independent checks give confidence that the hump mode is indeed present.

Because in 1942 performing flutter calculations by hand was such a laborious and time-consuming endeavor, it is likely that Theodorsen and Garrick chose a coarse spacing of 1/k in their

implementation of Solution Method 3 and missed the presence of the hump mode. This possibility is illustrated below.

Figure 12(a) contains a raw form recomputation using Solution Method 3 and corresponds to the condition  $\frac{\omega_{\beta}}{\omega_{\alpha}} = 0.4$  in figure 11. For this recomputation 1001 values of 1/k were employed with a logarithmic distribution between 1/k = 0.01 and 1/k = 1000. In this plot, the three intersections identified by the dashed circles indicate the single flutter mode at  $\frac{\omega_{\beta}}{\omega_{\alpha}} = 0.4$  in figure 11(a) and the hump mode at  $\frac{\omega_{\beta}}{\omega_{\alpha}} = 0.4$  in figure 11(b).

It is not known how many values of 1/k Theodorsen and Garrick employed in their raw form result using Solution Method 3. But, as an illustration of how easy it would be to miss the hump mode, if they had chosen 15 values of 1/k ranging between 0.01 and 5, with a logarithmic distribution, they would have produced the recomputed result shown in figure 12(b). They would have predicted the single flutter mode but completely missed both the destabilizing and restabilizing extremes of the hump mode.

#### 7 CONCLUDING REMARKS

In the year 2000 in an AIAA Journal of Aircraft Engineering Note, Zeiler made generally known that three foundational NACA reports by Theodore Theodorsen and I.E. Garrick and two early aeroelasticity texts addressing aeroelastic flutter contained numerical errors in some of their numerical examples. Zeiler recommended that an effort be undertaken to employ the computational resources available today (digital computers) to recompute the numerical examples in these early works and to publish the results so as to provide a complete and error-free set of numerical examples.

A multiyear effort is underway that follows Zeiler's recommendation by re-computing the numerical examples in these three NACA reports and comparing the recomputations with the original results. For each NACA report, the recomputations were performed in Matlab® using the solution method particular to that report and spot-checked with modern flutter solution methods (also performed in Matlab®). Agreement between the recomputed results and spot-checks was excellent, providing confidence that the recomputed results were correct, especially in those instances where the original results and recomputed results differed significantly. To date the recomputations and comparisons with the original results have been completed for two of the NACA reports and have begun for the third.

The present paper has assembled representative examples of these comparisons. With some notable exceptions, given that the original results were obtained "by hand" with pencil, paper, slide rules, and mechanical calculators called comptometers, the recomputed and original results agreed astoundingly well in magnitude, in the shapes of the curves, and in the trends with variations in parameters. The notable exceptions are attributed to suspected errors in the original results.

#### **REFERENCES**

- [1] Theodorsen, Theodore: General Theory of Aerodynamic Instability and the Mechanism of Flutter. NACA Report No. 496, 1940.
- [2] Theodorsen, Theodore; and Garrick, I. E.: *Mechanism of Flutter, a Theoretical and Experimental Investigation of the Flutter Problem.* NACA Report No. 685, 1940.
- [3] Theodorsen, Theodore; and Garrick, I. E.: Flutter Calculations in Three Degrees of Freedom. NACA Report No. 741, 1942.
- [4] Zeiler, Thomas A.: *Results of Theodorsen and Garrick Revisited*. Journal of Aircraft. Vol. 37, No. 5, Sept-Oct 2000, pp 918-920.
- [5] Bisplinghoff, R. L.; Ashley, H.; and Halfman, R. L.: *Aeroelasticity*, Addison-Wesley-Longman, Reading, MA, 1955.
- [6] Bisplinghoff, R. L.; and Ashley, H.: *Principles of Aeroelasticity*, Dover, New York, 1975.
- [7] Perry, Boyd III: *Re-Computation of Numerical Results Contained in NACA Report No. 496*. NASA TP-2015-218765, June 2015.
- [8] Perry, Boyd III: *Re-Computation of Numerical Results Contained in NACA Report No. 685*. NASA TP in process.
- [9] Dickson, Leonard Eugene: First Course in the Theory of Equations. John Wiley & Sons, Inc., 1922. (Reprinted by Petra Books, www.petrabooks.com)
- [10] Hassig, Hermann J.: An Approximate True Damping Solution of the Flutter Equation by Determinant Iteration. Journal of Aircraft, Vol. 8, No. 11, November 1971, pp. 885-889.
- [11] Abel, Irving: An Analytical Technique for Predicting the Characteristics of a Flexible Wing Equipped with an Active Flutter-Suppression System and Comparison with Wind-Tunnel Data. NASA TP 1367, February 1979.
- [12] Brunton, Steven L.; and Rowley, Clarence W.: *Empirical State-Space Representations for Theodorsen's Lift Model*. Journal of Fluids and Structures, Vol. 38, April 2013, pp. 174-186.

#### **COPYRIGHT STATEMENT**

The authors confirm that they, and/or their company or organization, hold copyright on all of the original material included in this paper. The authors also confirm that they have obtained permission, from the copyright holder of any third party material included in this paper, to publish it as part of their paper. The authors confirm that they give permission, or have obtained permission from the copyright holder of this paper, for the publication and distribution of this paper as part of the IFASD-2019 proceedings or as individual offnumber-prints from the proceedings.

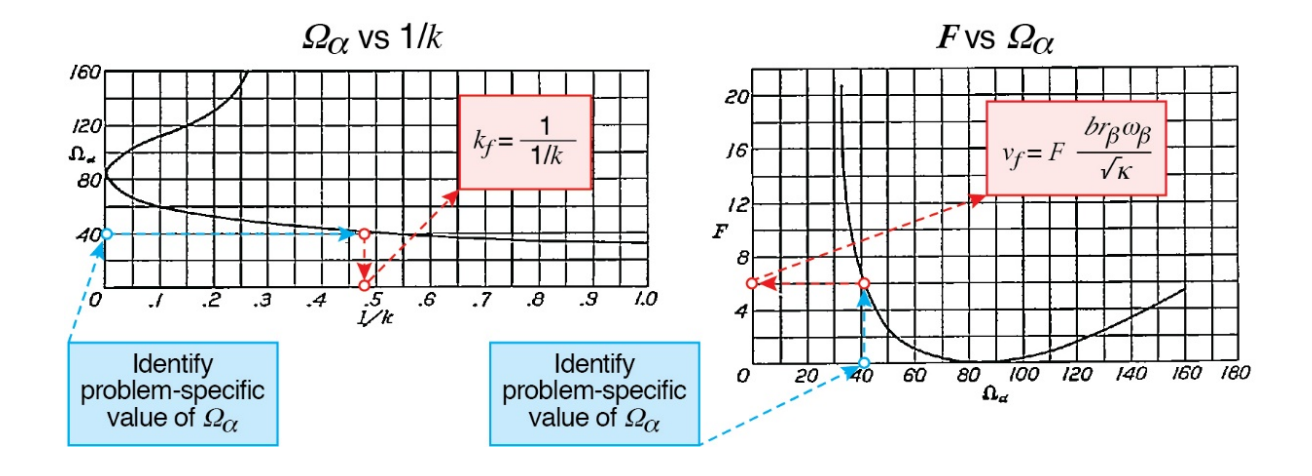


Figure 1. – Example of Solution Method 1 from *NACA 496*, figs. 5 and 6, Case 3 (torsion-aileron).

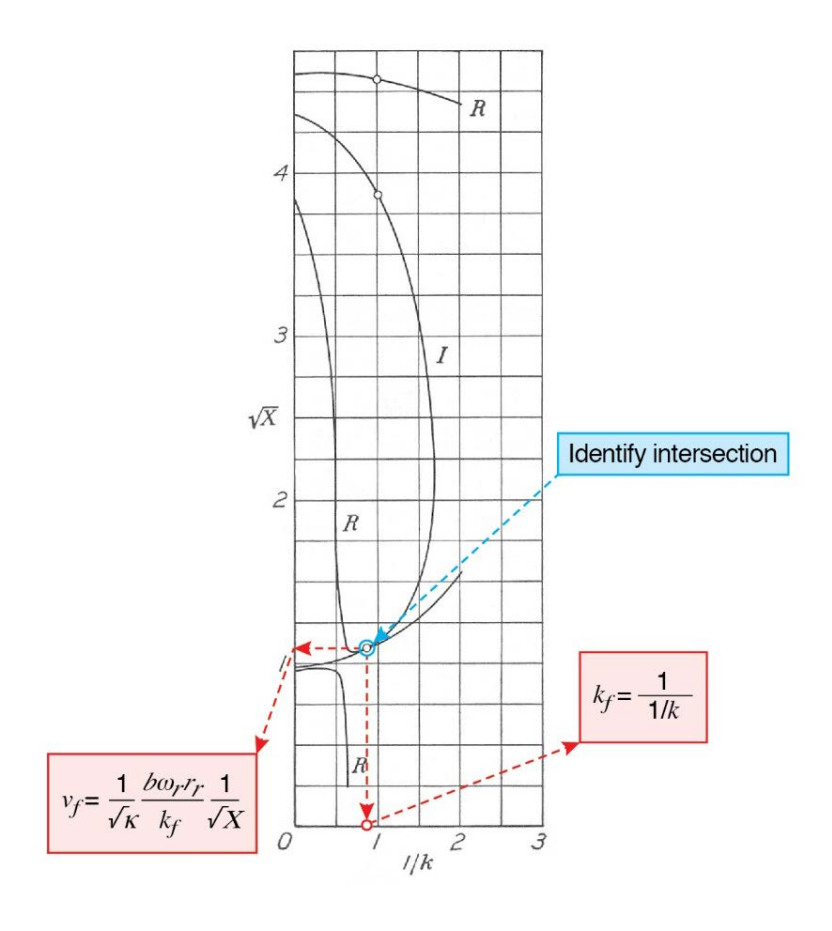


Figure 2. – Example of Solution Method 2 from NACA 685, fig. 4, 3DOF.

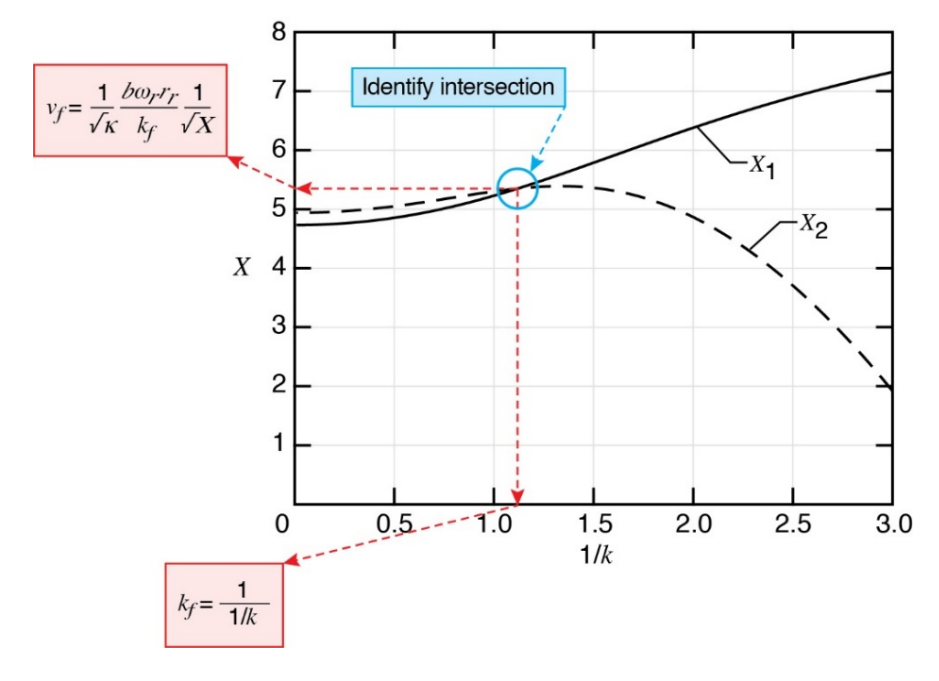


Figure 3. – Example of Solution Method 3, corresponding to  $x_{\beta}=0.004$  and  $\frac{\omega_{\beta}}{\omega_{\alpha}}=1.4$  in fig. 1 of *NACA 741*, 3DOF.

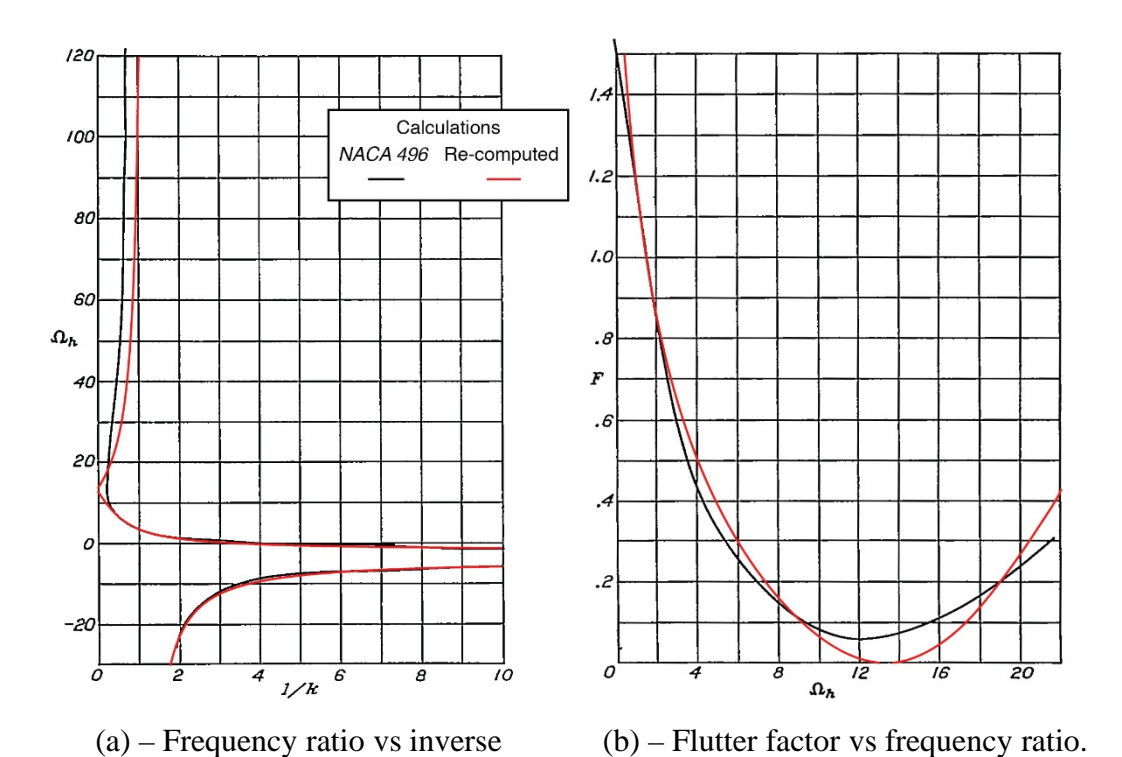


Figure 4. – Comparison of original and recomputed results *NACA 496*, figs. 9 and 10, Case 1 (flexure-torsion).

of reduced frequency.

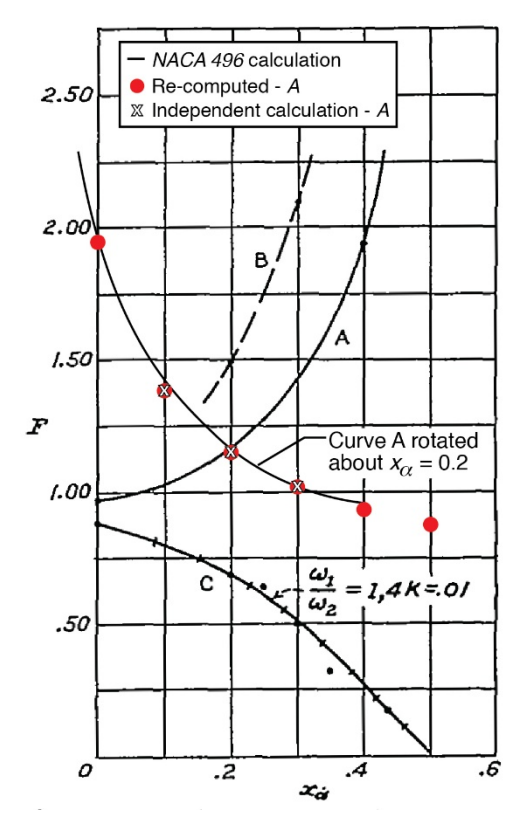


Figure 5. – Comparison of original and recomputed results *NACA 496*, fig. 14, Case 1 (flexure-torsion).

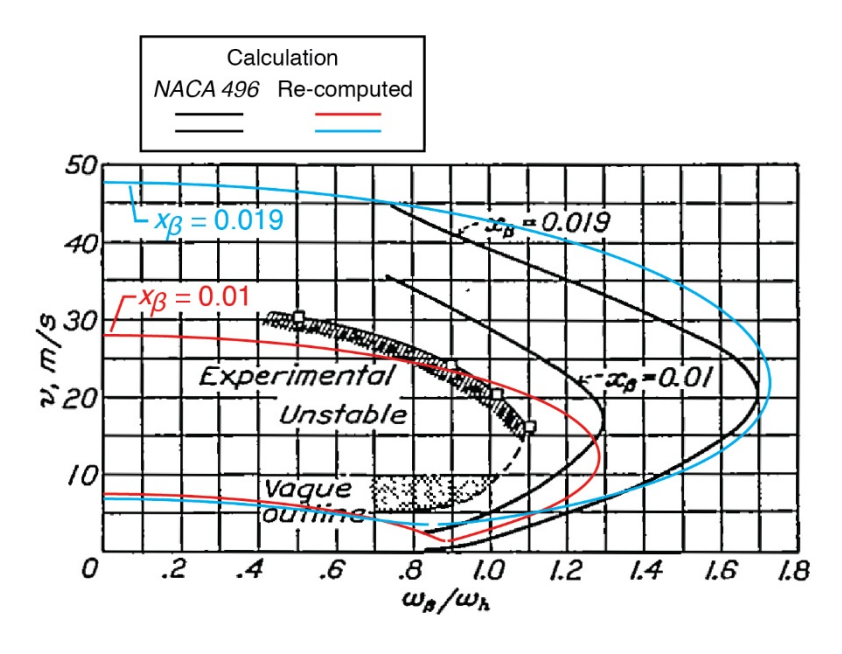


Figure 6. – Comparison of original and recomputed results *NACA 496*, fig. 16, Case 2 (aileron-flexure).

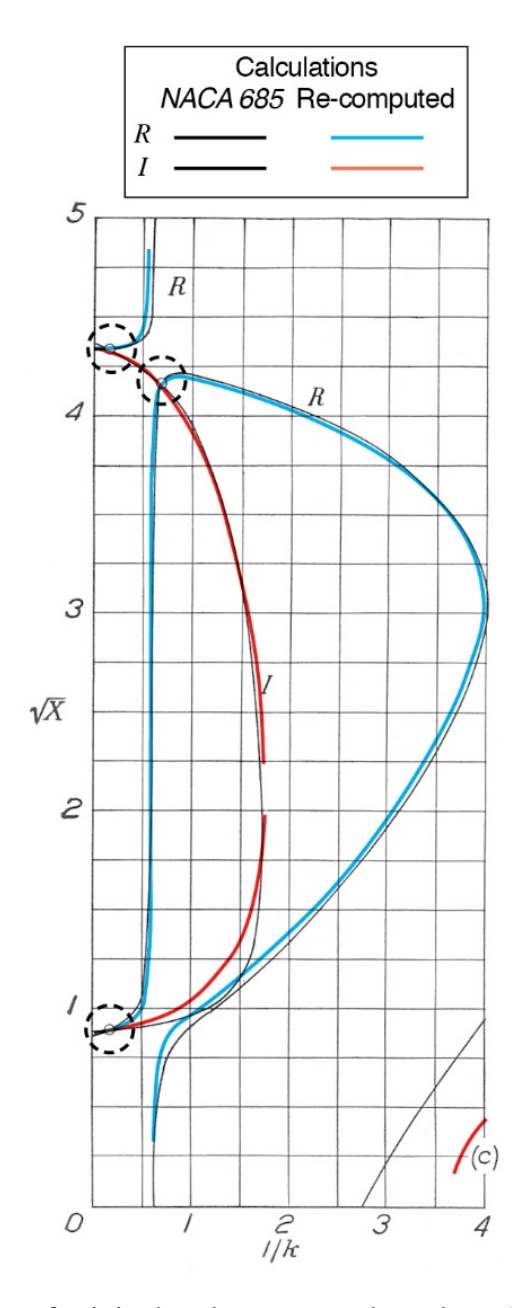


Figure 7. – Comparison of original and recomputed results *NACA 685*, fig. 7(c), 3DOF. Dashed circles indicate intersections of real and imaginary loci.

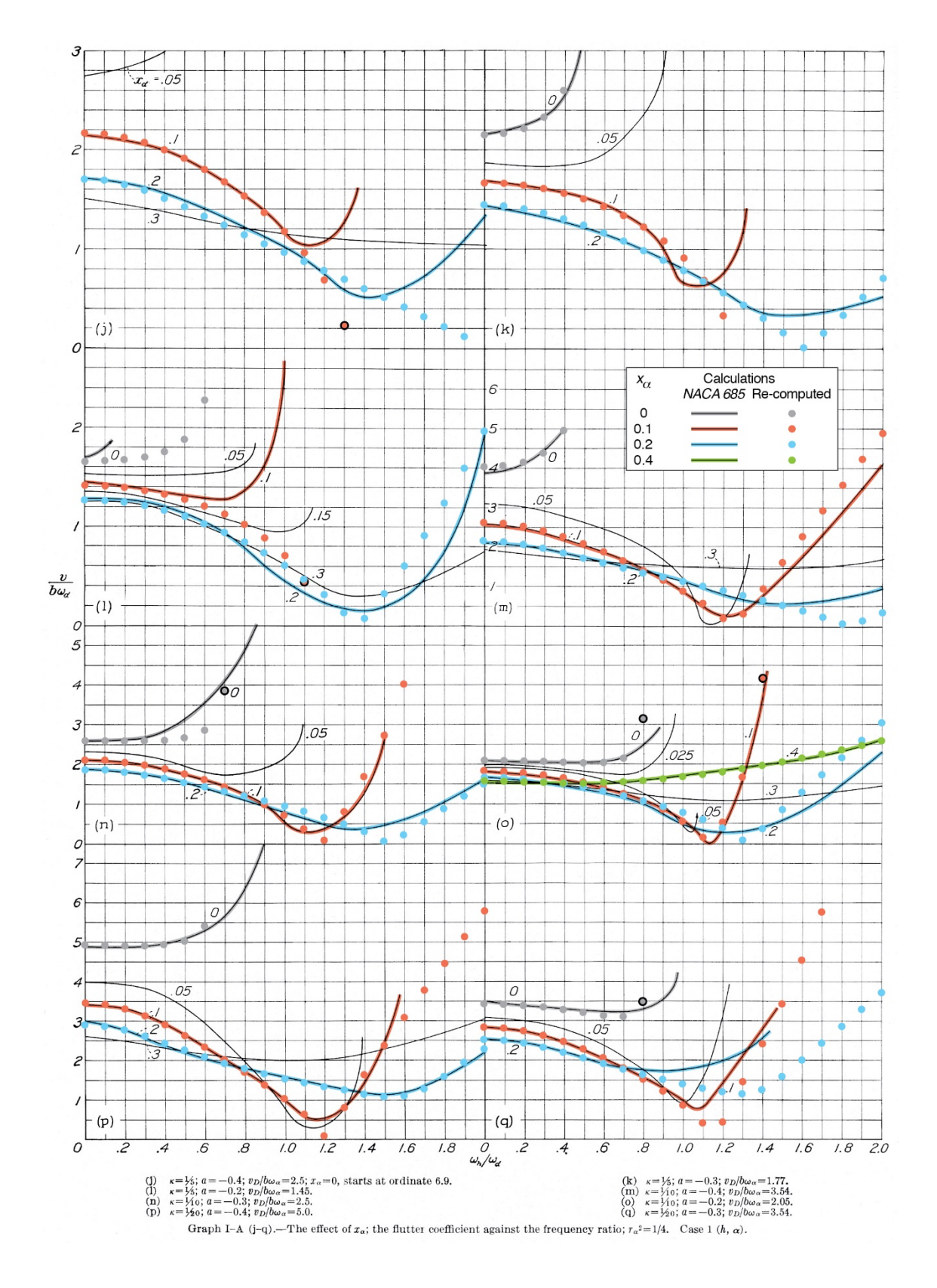


Figure 8. – Comparison of original and recomputed results *NACA 685*, Graph I-A, parts (j) to (q), Case 1 (flexure-torsion).

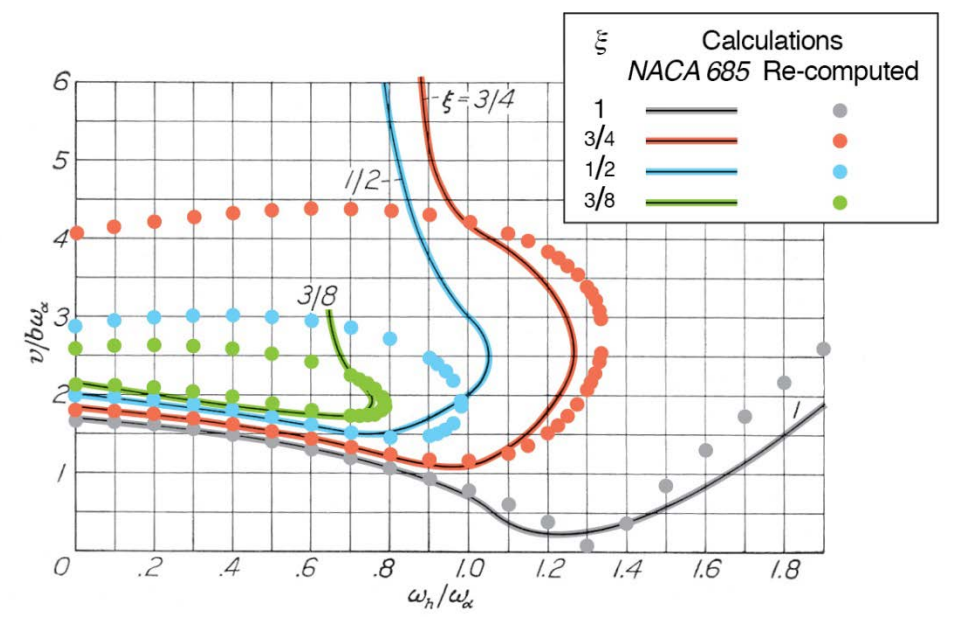


Figure 9. – Comparison of original and recomputed results *NACA 685*, Graph I-G, Case 1 (flexure-torsion).

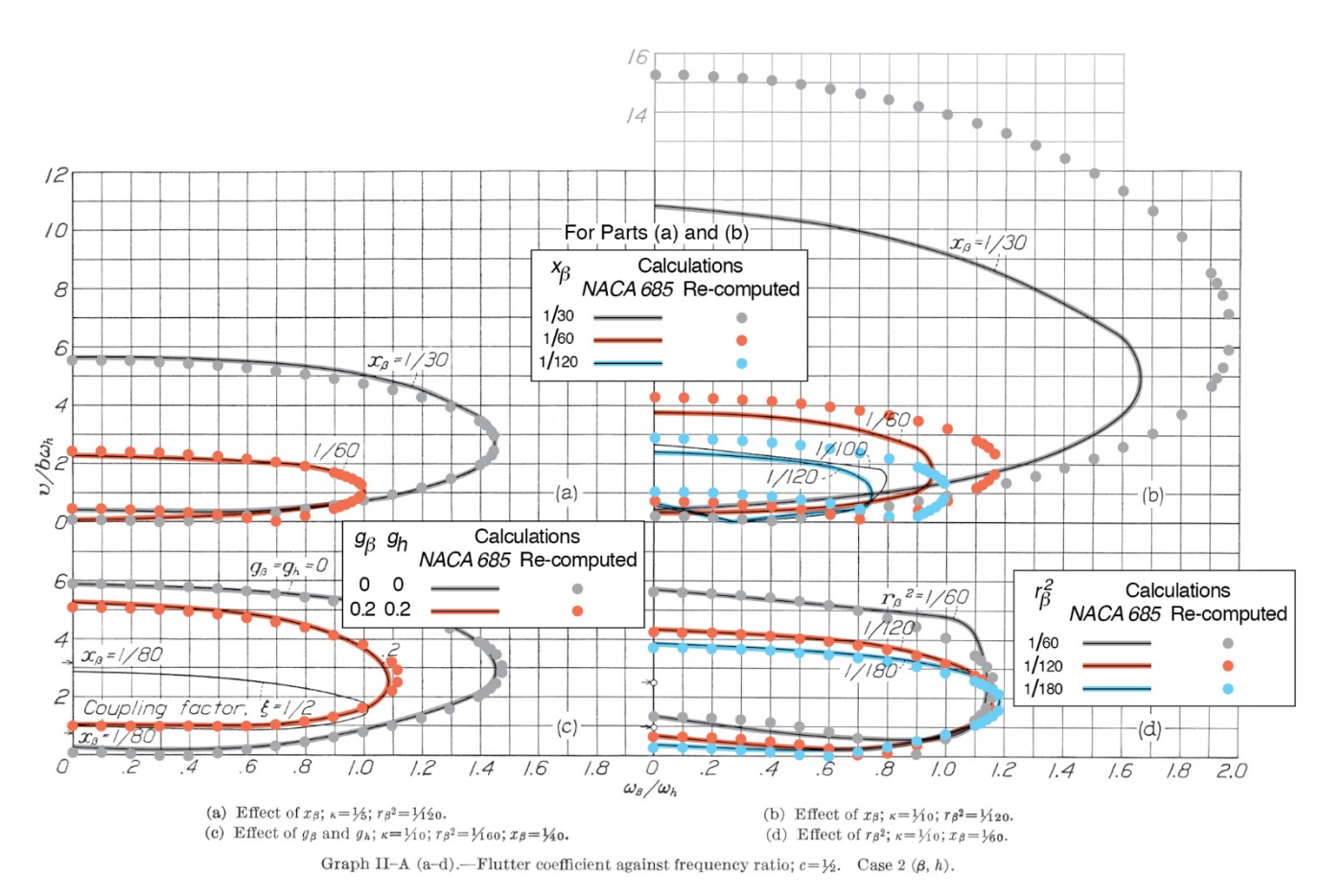
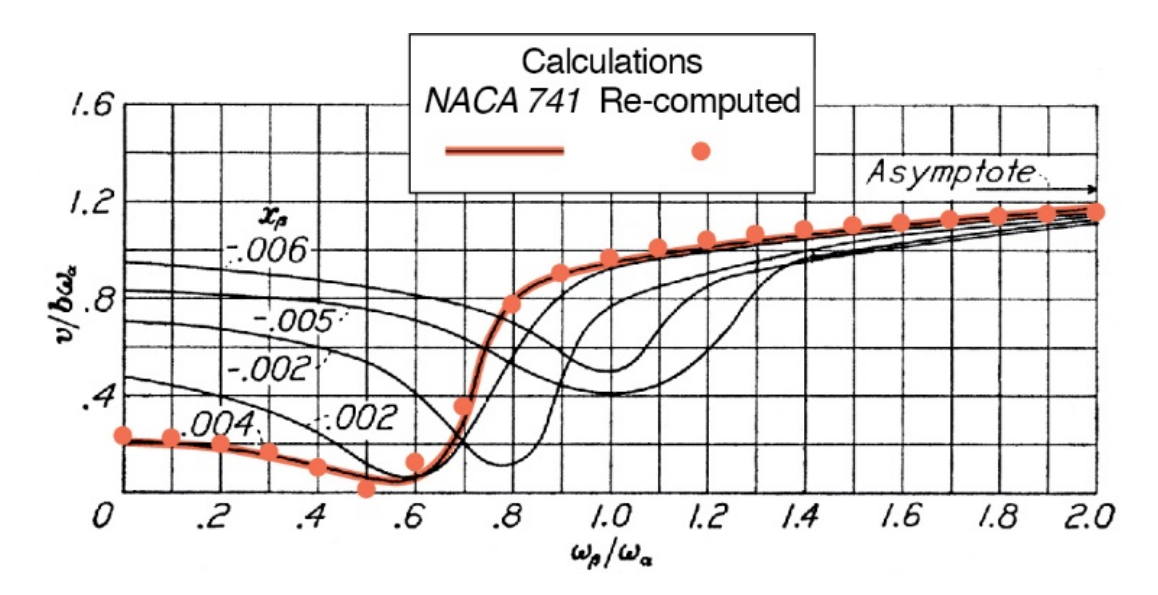


Figure 10. – Comparison of original and recomputed results *NACA 685*, Graph II-A, Case 2 (aileron-flexure).



(a) – Single flutter mode.

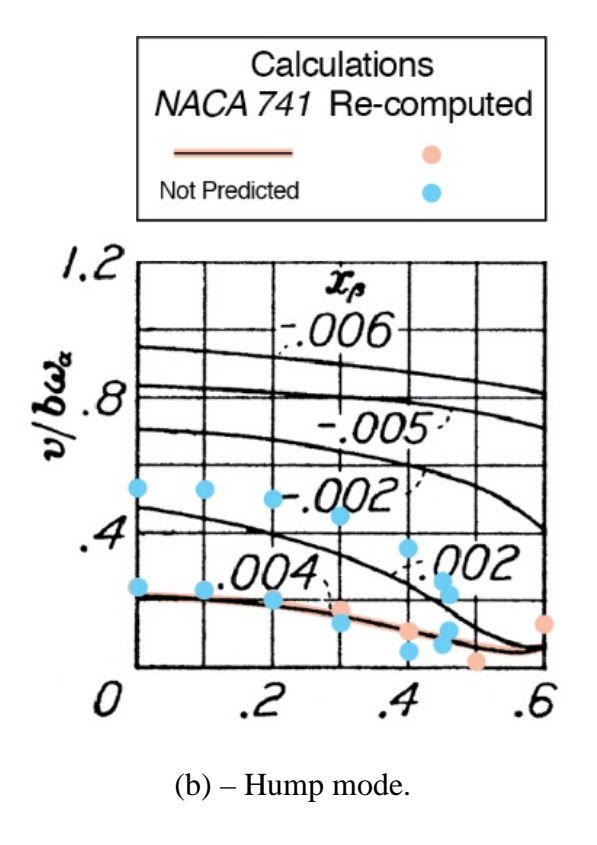
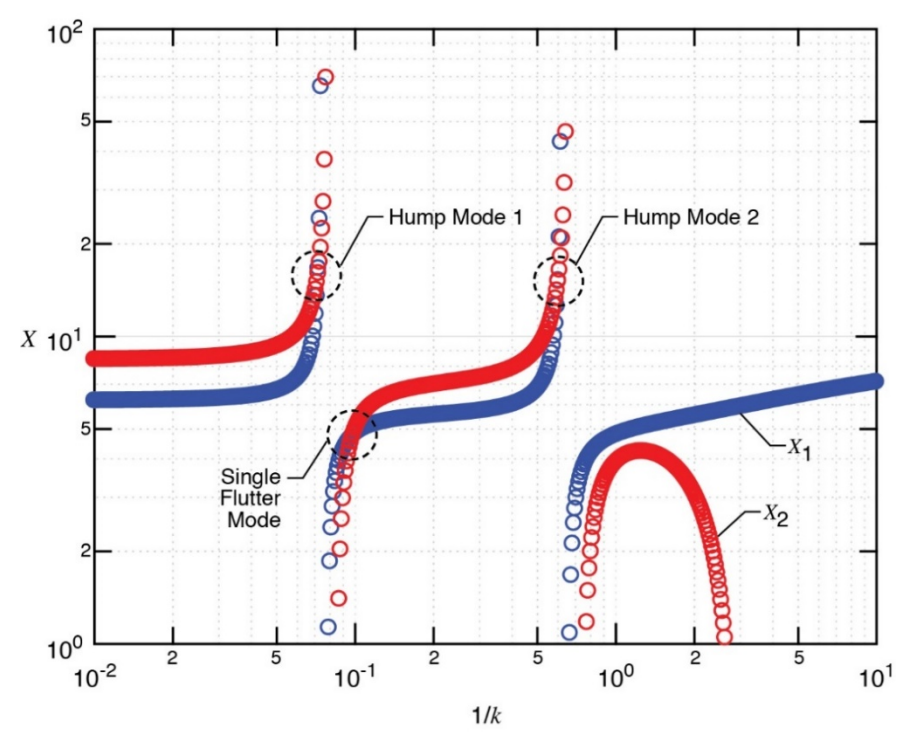
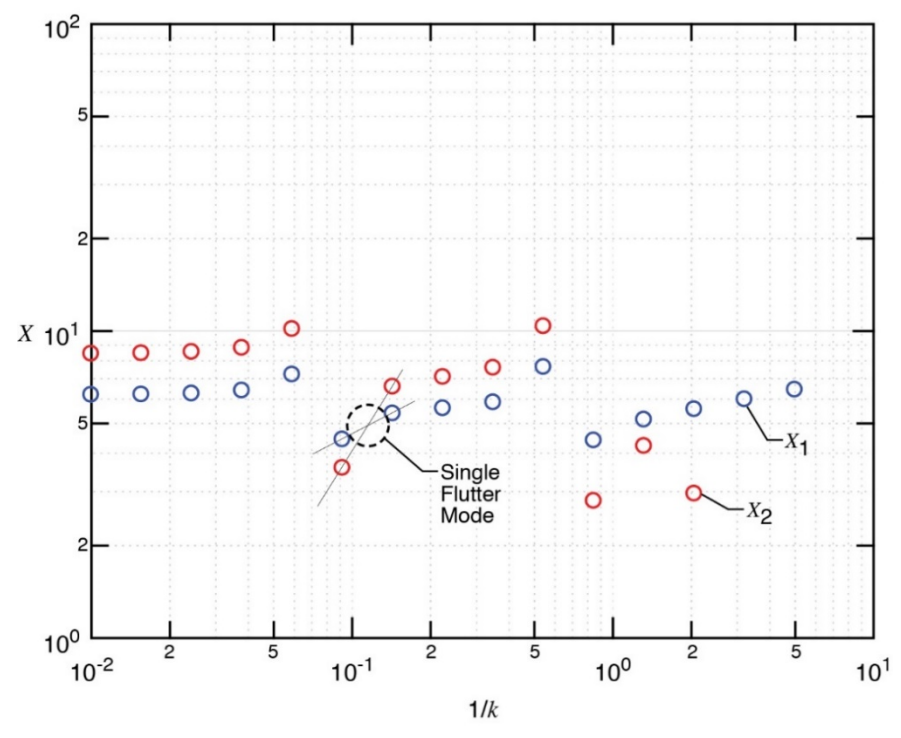


Figure 11. - Comparison of original and recomputed results NACA 741, fig. 1, 3DOF.



(a) -1001 values of 1/k ranging from 0.01 to 1000



(a) -15 values of 1/k ranging from 0.01 to 5

Figure 12. – Recomputation of result from *NACA 741*, fig. 1,  $x_{\beta}=0.004$ ,  $\frac{\omega_{\beta}}{\omega_{\alpha}}=0.4$ , 3DOF.